Electric Power Systems Research 218 (2023) 109212

Contents lists available at ScienceDirect

Electric Power Systems Research

journal homepage: www.elsevier.com/locate/epsr

A method for detecting conductive droplet deformation and flashover using interface temperature based on electrothermal synergistic mechanism

Jikai Bi [a], Yanpeng Hao [a,*], Yashuang Zheng [a,*], Xiaoxiang Wu [a], Haixin Wu [a], Lei Huang [a], Yanwen Chen [a,b], Lin Yang [a]

[a] School of Electric Power Engineering, South China University of Technology, Guangzhou 510640, China
[b] School of Electrical and Information Engineering, Anhui University of Science and Technology, Huainan 232000, China

ARTICLE INFO

Keywords:
Droplet deformation
Flashover
Interface temperature
Surface temperature
Electrothermal synergistic mechanism

ABSTRACT

Deformation and discharge of water droplets on composite insulator surface are usually accompanied by heat change. This paper aims to seek a method for monitoring droplet appearance and flashover discharge based on interface temperature. It is expected to obtain electrothermal synergistic mechanism in the process of dynamic deformation and discharge of droplets. Fiber Bragg gratings were embedded at the interface of silicone rubber–epoxy resin plate specimen to measure interface temperature. A comprehensive test platform of water droplets was established to detect droplet appearance, UV photon number, leakage current and surface infrared temperature. Formation mechanism of high temperature points on hydrophobic surface during droplet deformation was proposed. Test results show that leakage current could hardly reflect the droplet appearance. The sudden increase of droplet elongation is accompanied by surface temperature rise. A high temperature point appears near the elongated droplet in electric fields. The maximum surface temperature rise is 3.8 °C. As droplet appearance changes or flashover occurs, interface temperature increases. Temperature rise rate during the two stages are 1.19×10^{-3}~1.68×10^{-3} °C/s and 4.46×10^{-2}~5.77×10^{-2} °C/s, respectively. This paper is of great significance for improving the deformation and discharge mechanism of water droplets on the hydrophobic composite insulator surface.

1. Introduction

Green and low-carbon offshore wind power has developed rapidly in recent years. Silicone rubber insulators have been widely used in coastal transmission lines on account of unique advantages such as excellent hydrophobicity and anti-pollution flashover performance [12]. Compared with inland areas, coastal areas are characterized by high humidity and high salt content in fog. Discrete water droplets with high electrical conductivity tend to form on the surface of hydrophobic composite insulators [3]. Droplets greatly enhance the electric field between the silicone rubber surface, droplets and the air [4–6]. In electric fields, water droplets on the insulator surface will appear dynamic behaviors such as oscillation, deformation, fusion and movement, which may strengthen the surface electric field strength. Once the electric field strength reaches the breakdown strength of the air, surface discharge will occur and even develop into insulator flashover, seriously affecting the safe and stable operation of transmission lines [7–9].

The dynamic behavior of water droplets on the surface of hydrophobic silicone rubber has drawn extensive attention from scholars. Water droplets on the composite insulator surface will oscillate in AC electric fields. The oscillation is divided into three stages: (1) At the initial stage of applying voltage, the top of water droplets oscillates irregularly by polarization. (2) As applied voltage rises, it develops into the oscillation of the whole water droplet. The clear peak and valley of water droplets appear. (3) Before the critical flashover, the water droplet oscillates left and right under the action of Coulomb force. The frequency changes from double working frequency in the first two stages to the working frequency [10]. Adamiak et al. [11] pointed out that there was a critical field strength. Water droplets only oscillate when the electric field is less than the critical value. As it reached to the critical field strength, the water droplet begins to deform. The deformation is divided into three stages: elongation of water droplets, formation of a neck in the middle of the water droplet and ejection of a thin jet from the droplet tip. Cao et al. [12] indicates that with the volume of water

* Corresponding authors.
E-mail addresses: yphao@scut.edu.cn (Y. Hao), zysscut@scut.edu.cn (Y. Zheng).

https://doi.org/10.1016/j.epsr.2023.109212
Received 3 November 2022; Received in revised form 20 January 2023; Accepted 8 February 2023
Available online 13 February 2023
0378-7796/© 2023 Elsevier B.V. All rights reserved.

droplets increases, the distortion rate decreases and the elongation rate increases. The increase of the elongation and volume of water droplets leads to more serious electric field distortion. Meanwhile, the amplitude of deformation factor and elongation factor shows increasing tendency with an increase in electric field strength.

Water droplets may fuse with each other. The fusion first occurs between larger size droplets. With the increase of electric field strength, the probability of water droplet fusion increases and the fusion phenomenon on the high-voltage side is more serious. Increased fractal dimension of water droplets makes water droplet distribution be more complex and irregular, resulting that the fusion is hard to happen. While, the maximum electric field strength around the water droplet shows an increasing tendency, leading to an increased likelihood of surface discharge [6].

In addition, the impact of droplet parameters such as volume, number, conductivity and viscosity on the surface discharge and insulator flashover also attracts the interest of scholars. Cao et al. [13] put forward that there was a critical water proportion for a given dry band length and droplet conductivity. Below the critical water proportion, the flashover voltage generally decreases with the increase of the water volume and droplet number. The occurrence of partial arc would definitely lead to the flashover. Li et al. [14] revealed that with the increase of droplet volume and conductivity, the droplet elongated and the flashover voltage decreased. Chatterjee and Nazemi [15] found that droplets with high viscosity would enhance the resistance to the droplet movement and hinder the droplet deformation, resulting in a higher discharge inception voltage.

The water droplet morphology on the hydrophobic silicone rubber surface is closely related to the electric field distribution, discharge inception voltage and flashover voltage. Deformation of water droplets is a necessary condition for surface discharge. Insulator discharge and flashover are not only electrical process, but also thermal process [16]. Loberg et al. [17] established a function between the surface resistivity and temperature distribution across the hydrophilic insulating surface. During the formation of dry band on the surface of hydrophilic polluted glass sample, Guan et al. [18] used an infrared thermal imager to record the temperature distribution. Dry band first appears in the high temperature zone. It develops with the extension of the high temperature zone on the pollution layer surface. Hao et al. [19] implanted fiber Bragg gratings (FBGs) at the silicone rubber–epoxy resin interface. The starting time of interface temperature rise detected by interface FBGs lags 1.4 s behind surface leakage current. Subsequently, FBGs were implanted at the insulator housing–core rod interface to make fiber composite insulators. As arc discharge occurred on the insulator surface, a new phenomenon of a sharp drop before a rapid increase in interface temperature was observed [20]. Three characteristic quantities of Euclidean Distance (the measuring standard for the otherness of interface temperature of different axial positions), a sharp drop in interface temperature and interface temperature rise were proposed to monitor the dry band arc on the composite insulator surface [21]. The feasibility of using FBGs to detect dry band arc on the surface of online composite insulators was discussed. The influence of various stresses and ambient temperature on the detection results was eliminated.

Some achievements about the relational characteristics between the temperature and surface appearance of hydrophilic insulators have been acquired. However, there are very few studies on the temperature characteristics of water droplet morphology, water droplet discharge and flashover on the hydrophobic insulator surface. Rowland et al. [22] used spectral emission method to measure the arc temperature as the discharge occurred between water droplets with small current. Xie et al. [2324] recorded the temperature of water droplets at the initial stage of discharge arc by an infrared thermal imager. The discharge path was from high potential droplets to low potential droplets. The temperature rise of low potential droplets was higher. The temperature in above references was measured when the surface discharge occurred. While, temperature characteristics during water droplet deformation process before surface discharge have not been researched yet.

In this paper, fiber Bragg gratings (FBGs) were implanted at the interface of hydrophobic silicone rubber and epoxy resin flat specimen. Discharge test was carried out on the specimen with linearly arranged water droplets on the surface. During the dynamic water droplets deformation, elongation of water droplets, UV photon number, leakage current, surface infrared temperature and interface grating temperature were measured. The relationship between the state of water droplets and temperature was explored. The interface temperature and surface temperature were used to detect and characterize the surface insulation state of hydrophobic silicone rubber.

2. Materials and methods

2.1. Detecting system

The test and detection system in this paper includes power supply, FBG demodulator, infrared thermal imager, ultraviolet imaging meter, leakage current acquisition device, surveillance camera and silicon rubber–epoxy resin flat specimen, as shown in Fig. 1(a). The power transformer with rated capacity of 250 kVA, rated voltage of 50 kV, rated current of 5 A, the maximum short circuit current of 75 A, working frequency of 50 Hz, short-circuit impedance of ≤2%, output voltage waveform distortion rate of <3%, which meet the requirements of IEC 60,507 [25] for AC contamination test power supply, was applied as the experimental power supply. FBG demodulator with the type of JEME-iFBG-S08, wavelength sensitivity of 0.1 pm and scanning frequency of 10 Hz was used to detect the interface temperature of the specimen. The infrared thermal imager with the type of HIKMICRO TP96 and measuring range of -20 °C ~ 650 °C was used to detect the surface temperature. The ultraviolet imaging meter with the type of DayCor Superb, the sensitivity of 1 pC and the gain of 110 times was used to detect the surface discharge intensity. The leakage current collection device is a series resistance type device. The collection card model is USB3106. The frame rate of the surveillance camera is 30 fps and the exposure time is 10 ms. It should be noted that the sample in Fig. 1(a) is represented in top view for visual effect.

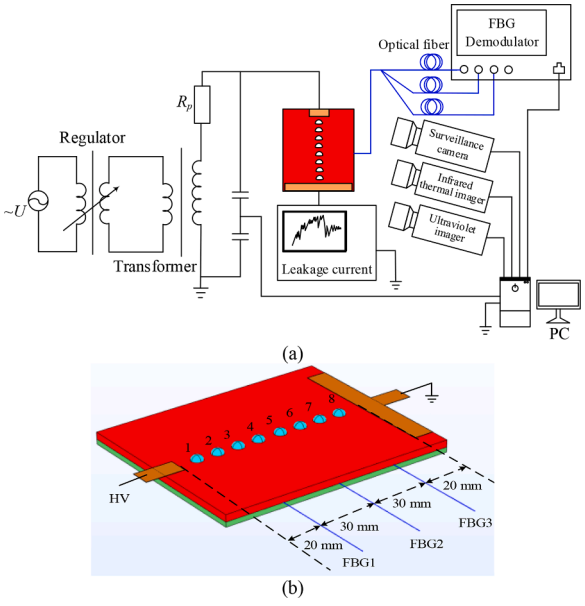


Fig. 1. The test and detection system for the water droplet discharge on the silicone rubber surface. (a) Detecting system, (b) Distribution of water droplets, and FBGs.

2.2. Specimen and method

The thickness of the specimen is 4 mm and the distance between two electrodes is 100 mm. 8 water droplets with the size of about 50 μL and the conductivity of 20 mS/cm were set on the specimen surface. They are numbered respectively as droplet 1 to droplet 8, as shown in Fig. 1 (b). Fig. 1(b) also shows that three FBGs are embedded at silicone rubber–epoxy resin interface. The grating FBG2 is located in the middle of the specimen, FBG1 is 20 mm away from the high-voltage electrode and FBG3 is 20 mm away from the ground strap. Grating parameters are given in Table 1. λ denotes the wavelength range, L denotes the grating length, T denotes range of operating temperature, d denotes the diameter of the fiber cladding and δ denotes diameter of the fiber core.

The embedded fiber Bragg gratings named FBG1, FBG2 and FBG3 were used to detect the interface temperature, which was expected to express the state of water droplets on specimen surface. The temperature measurement principle of FBGs has described in literature [21].

2.3. Temperature calibration test of FBGs

The temperature coefficient of FBGs embedded at the specimen interface was measured in the thermostatic chamber. The test temperature in the thermostatic chamber was set as 0 °C, 10 °C, 15 °C, 20 °C, 25 °C, 30 °C and 40 °C successively. To make the temperature at embedded FBGs consistent with the temperature in the thermostatic chamber, the specimen was placed in the thermostatic chamber at the set temperature for more than 8 h before the central wavelength was recorded [26].

2.4. Applied voltage

AC voltage was applied to the specimen and held constant for at least 60 s. If there was no discharge occurred on the specimen surface, applied voltage would be increased. The applied voltage is shown in Fig. 2.

3. Results and analysis

3.1. Temperature coefficient K_T of interface FBGs

The wavelength shift of interface FBGs corresponding to different temperatures is shown in Fig. 3. It exhibits line relationship between the wavelength shift and the temperature. Temperature coefficients K_T are shown in Table 2. Temperature coefficients K_T of the interface FBG are diverse due to the influence of manufacturing process and the interaction between gratings and the silicone rubber, which may cause different thermal expansion of grating material. In spite of that, linear relationship between wavelength shift and temperature is valid for detecting the interface temperature.

3.2. Water droplet appearance

As the voltage is applied to the specimen, water droplets on the silicone rubber surface may elongate along the electric field direction due to the combined action of electric field force and surface tension. Fig. 4 shows the water droplet appearance. Droplet 1 and droplet 2 began to be significantly elongated along the electric field direction at about 600 s and 628 s respectively. During 1020 ~1200s, droplet 3 appeared significant deformation and elongation. At about 1200 s, droplet 3 started to move, as marked in Fig. 4. The surface of the specimen plate is not absolutely horizontal. The movement of droplet 3 may be due to the combined effect of the gravitational force of the water droplet sliding down the sloping surface of the specimen plate, surface tension and electric field force. It can be seen from the visible light images at 1392 s and 2760 s that the water droplet 2 was deformed from ellipsoid to triangle, and the semi-major axis was significantly reduced. It should be noted that the droplet elongation in this paper refers to the elongation along the horizontal direction of 8 water droplets. The droplet movement refers to the elongation along other directions.

Elongation rate η of water droplets on the specimen surface is [12]

$$\eta = (L - L_0)/L_0 \quad (1)$$

where L denotes the length of water droplets and L_0 denotes the initial length of water droplets. Based on image recognition technology, the elongation of water droplets during 0 ~1250 s was obtained, as shown in Fig. 5. It should be noted that the semi-major axis of water droplets does not always increase on account of the influence of water evaporation and water droplet deformation. In some cases, the semi-major axis

Table 1
FBG parameters of the optical fiber composite insulator.

Fiber Type	λ/pm	L/mm	T/ °C	d/μm	δ/μm
Acrylate SMF-28e	1510~1590	10	-40~300	300	8

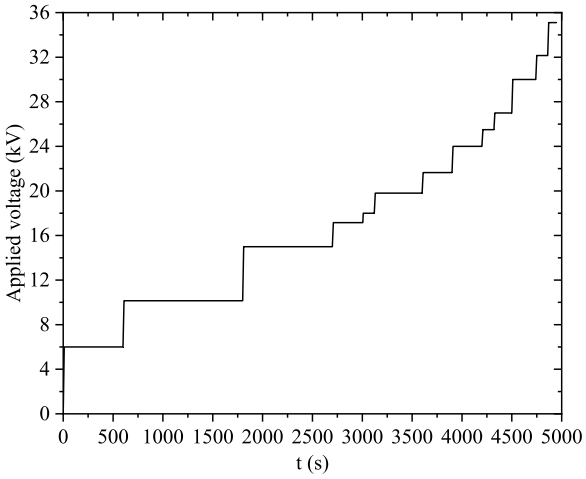


Fig. 2. Applied voltage.

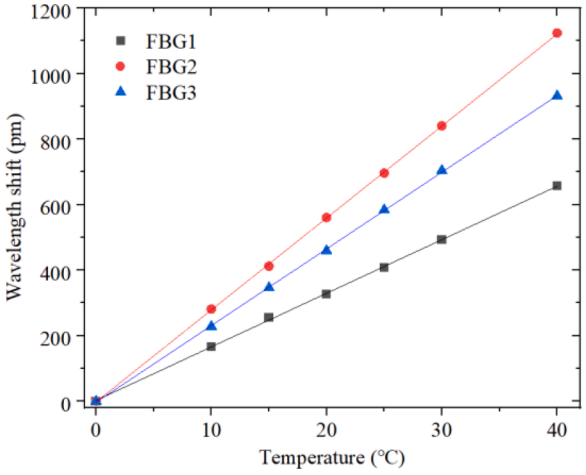


Fig. 3. The wavelength shift of interface FBGs corresponding to different temperatures.

Table 2
Temperature coefficients of FBGs at insulator core-sheath interface.

Fiber grating	FBG1	FBG2	FBG3
K_T (pm/ °C)	16.363	28.092	23.421

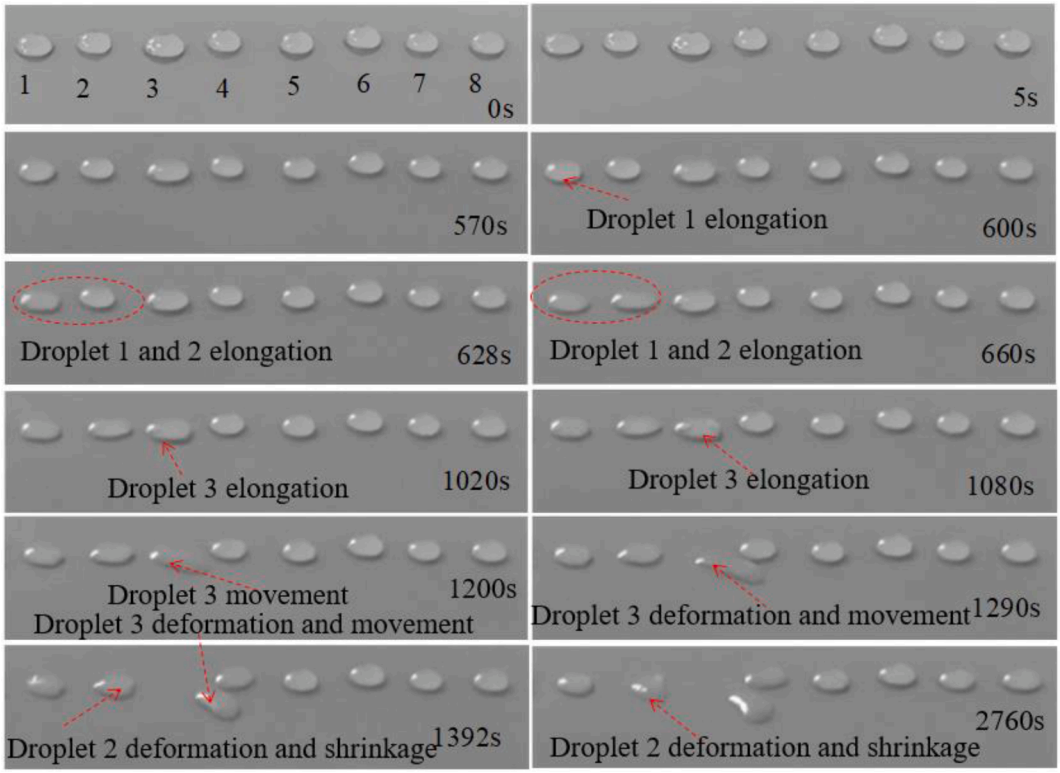


Fig. 4. The water droplet appearance on silicone rubber surface.

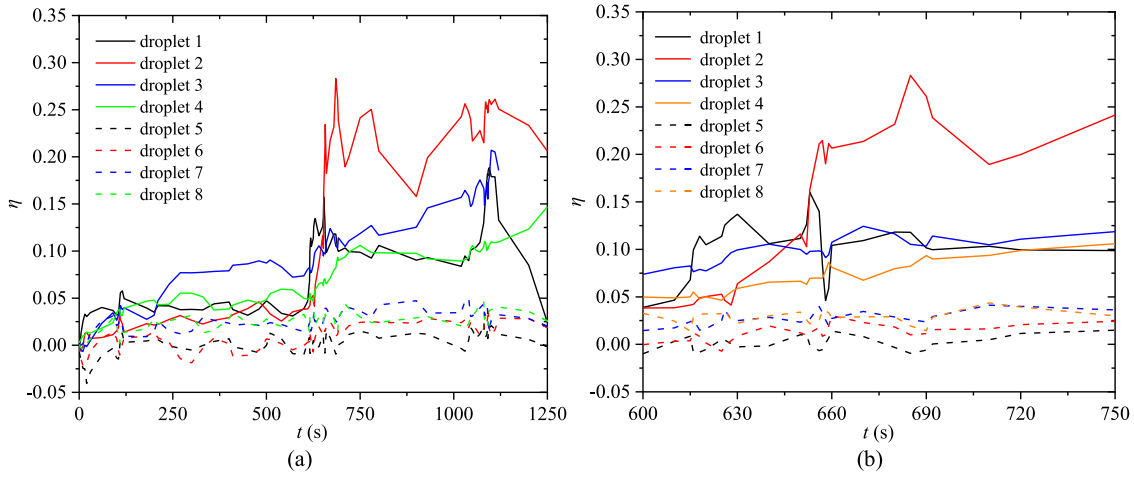


Fig. 5. Elongation rate of water droplets on hydrophobic silicone rubber surface in AC electric fields. (a) 0~1250s, (b) 600~750 s.

may be lower than its initial value (i.e. $\eta < 0$). As shown in Fig. 4, droplet 2 deformed and shrank. The semi-major axis of droplet 2 decreased significantly. In this paper, only the elongation during the first 1250 s with obvious water droplet elongation is given.

Applying voltage to the specimen, water droplets elongated along the electric field direction slowly. At about 600 s, elongation rate η of droplet 1 began to rise rapidly and the maximum elongation was about 0.19. At about 628 s, η of droplet 2 increased rapidly and the maximum elongation is about 0.32.

3.3. UV photon number

In AC electric fields, ultraviolet image and UV photon number of water droplets on hydrophobic silicone rubber surface are described in Fig. 6. At about 4420 s, corona discharge occurred between water droplet 1 and the high-voltage electrode with the photons number of 18,540, as shown in Fig. 6(a). UV photon number when corona discharge occurred is lower than that at 4010 s before corona. It may be that the ultraviolet discharge between the high-voltage electrode and high-voltage wire was serious at 4010 s, which affected the photon number of the specimen surface. No discharge sparks visible to the naked eye or captured by the camera were observed before the corona occurred at 4420 s. At about 4710 s, the corona discharge disappeared. From the elongation of droplet 1 to the occurrence of corona discharge, the surface water droplet has always been deformed. UV photon number in the process of droplet deformation and corona discharge is given in Table 3. In the process of droplet deformation, UV photon number is 220 ~23,400. The increase of photon number during this period may result from the continuous increase of applied voltage, which increases the surface electric field strength. In the process of corona discharge, UV

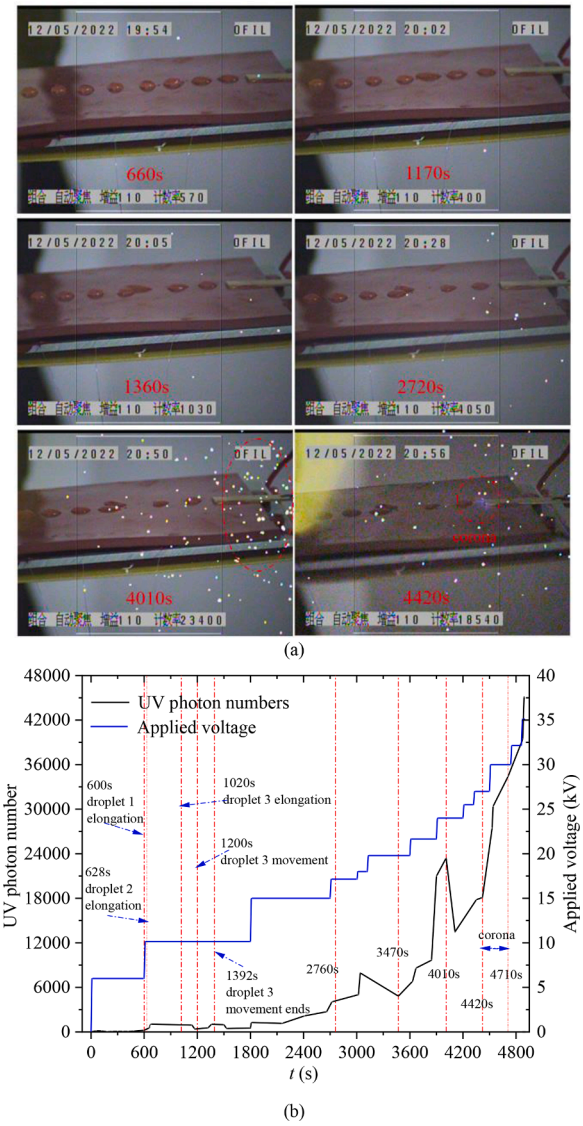


Fig. 6. Ultraviolet discharge of water droplets on hydrophobic silicone rubber surface in AC electric fields. (a) Ultraviolet image, (b) UV photon number.

Table 3
UV photon number in the process of droplet deformation and corona discharge.

Physical process	Droplet deformation	Corona discharge
UV photon number	220 ~23,400	18,540 ~34,410

photon number is 18,540 ~34,410.

3.4. Leakage current

The leakage current of water droplets on the hydrophobic silicone rubber surface in AC electric fields is shown in Fig. 7. There are no significant differences in the instantaneous values of leakage current between different stages such as 580~ 581 s, 4400~ 4401 s and 4850~ 4851 s. Before surface discharge of water droplets, the high-voltage electrode and the grounding electrode are insulated. The change of the resistance caused by the droplet deformation can be ignored. The surface state of the specimen cannot be judged from the leakage current.

3.5. Surface temperature

When an AC voltage was applied to the specimen, the infrared thermal imager was used to record the surface temperature of the specimen. The surface temperature in AC electric fields is shown in Fig. 8. High temperature points successively appeared on areas H-D1, D1-D2 and D2-D3. Area H-D1 denotes the position between the high-voltage electrode and droplet 1. Area D*m*-D*n* denotes the position between droplet *m* and droplet *n*. Both *m* and *n* represent a number from 1 to 8. The high temperature point in this paper refers to the area where surface temperature rises significantly.

Fig. 9 shows the maximum and minimum surface temperature of the specimen. The minimum temperature is the temperature of water droplets on the sample surface. Unless otherwise specified, surface temperature in this paper refers to the maximum surface temperature. Time points when water droplet state changes are given in Fig. 9 by dotted lines. The applied voltage is also described by the blue solid line.

From Fig. 8 and Fig. 9, the following information can be obtained.

Elongation stage of droplet 1 and droplet 2: at about 600 s, the maximum surface temperature started to rise rapidly. Bright high temperature points successively appeared on areas H-D1 and D1-D2. This is because droplet 1 and droplet 2 elongated rapidly along the electric field direction in turn. The surface heat production near droplet 1 and droplet 2 increased. At about 720 s, the maximum surface temperature basically remained unchanged. This may be due to the end of the rapid elongation process of droplet 1 and droplet 2.

Elongation stage of droplet 3: at about 1080s, the maximum surface temperature and water droplet temperature began to rise rapidly. A high temperature point appears on the area D2-D3, resulting from the elongation of droplet 3.

Movement stage of droplet 3: at about 1200s, droplet 3 began to move obviously. The maximum surface temperature and the water droplet temperature both rose. But the temperature rise is accompanied by several short drops. The movement of droplet 3 increased the dry band length of the specimen and changed the surface electric field. These changes made the electric field distribution more complex. Accordingly, the surface heat generation rate changed. The maximum surface temperature rose to 30.6 °C at about 1800 s. Subsequently, there

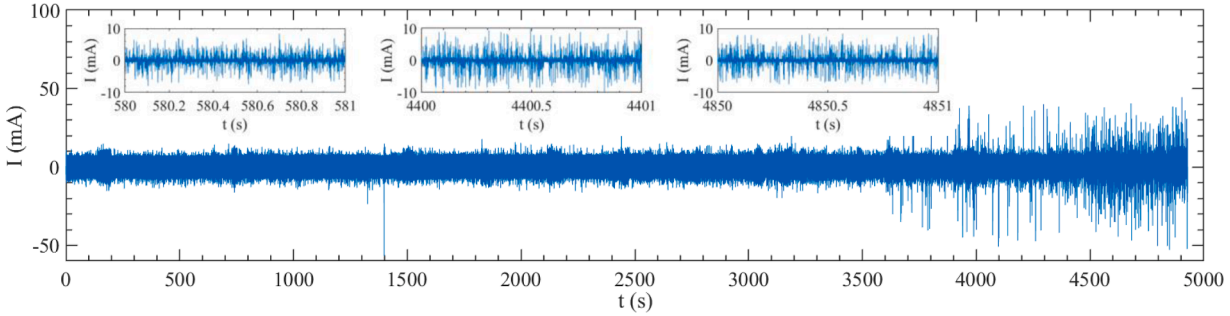


Fig. 7. Leakage current of water droplets on the hydrophobic silicone rubber surface in AC electric fields.

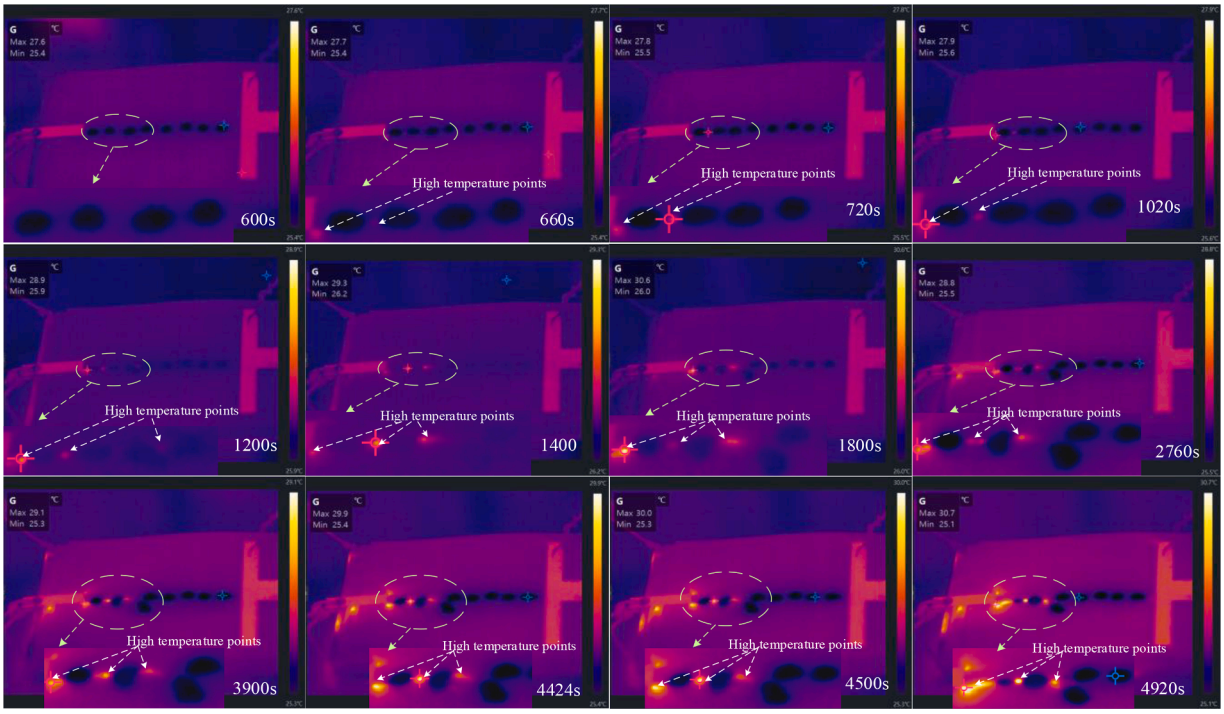


Fig. 8. Surface infrared temperature of the hydrophobic silicone rubber in electric fields.

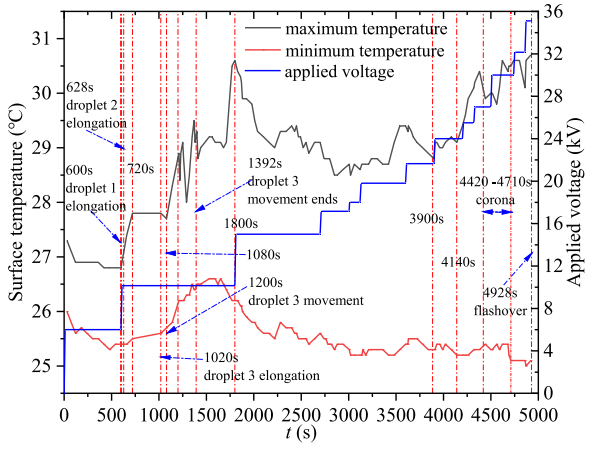


Fig. 9. The maximum and minimum surface temperature of the hydrophobic silicone rubber.

were still bright high temperature points on areas H-D1, D1-D2 and D2-D3. While, the maximum surface temperature started to drop. High temperature made the surface water evaporate and took away a mass of heat. The size of water droplets decreased, the length of dry band increased and the electric field strength decreased. Ultimately, the heat generation decreased.

Corona discharge stage: at 4420 s, a blue purple corona discharge appeared on the area H-D1. Table 4 shows that the maximum surface temperature rise in the process of corona discharge is only 0.9 °C, which is less than the temperature rise of 3.8 °C in the process of droplet deformation. It may be that corona discharge improved the electric field distribution and reduced the influence of corona heat generation on surface temperature. In addition, the surface temperature rose before the corona discharge appeared, which may be affected by the serious discharge between the high-voltage electrode and the high-voltage wire.

Table 4
Maximum surface temperature rise in the process of droplet deformation and corona discharge.

Physical process	Droplet deformation	Corona discharge
Maximum surface temperature rise / °C	3.8	0.9

3.6. Interface temperature

Interface temperature of the specimen in AC electric fields is described in Fig. 10. The time point when droplet appearance changes is given in Fig. 10 by the dotted line. The figure also shows the applied voltage by the orange solid line. At the initial stage of applying voltage to the specimen, the interface temperature decreased. This may result from the decrease of surface temperature caused by heat absorption in the process of droplet evaporation. In the previous study [20], the phenomena of water evaporation and interface temperature drop were also observed when arc discharge occurred on the moist pollution layer.

Elongation stage of droplet 1 and droplet 2: interface temperature was still decreasing. When surface heat is transferred to the interface

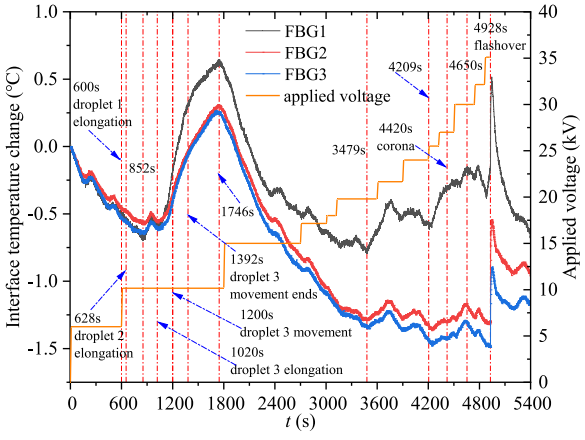


Fig. 10. Interface temperature change of the hydrophobic silicone rubber.

with lower temperature, it experiences loss and progressive decrease. The heat may have been completely dissipated before it is transferred to the interface. In addition, there is a time lag in temperature transfer. At about 852 s, the interface temperature decreased to the lowest value and then started to rise.

Elongation stage of droplet 3: interface temperature rose rapidly, reached to the maximum value at 1746s. Then it started to drop.

At 3479 s, the FBG1 interface temperature dropped to its lowest value. The high surface temperature led to water evaporation, a shorter droplet length, an increase in the length of the dry band and a change in electric fields. These caused the change of heat generation rate and the decrease of temperature. The increase in interface temperature after 3479 s is due to the increase in heat production as a result of the continued increase in applied voltage.

Corona stage: The interface temperature increased slowly with a relatively small temperature rise.

During the droplet deformation and flashover phases, interface temperature undergoes two significant rises. Table 5 describes the interface temperature change in the process of droplet deformation and flashover. The characteristics of the temperature rise are obviously different. During 1020 ~1740 s, temperatures of FBG1, FBG2 and FBG3 increase by 1.20 °C, 0.85 °C and 0.86 °C, respectively, with increase rates of 1.68 × 10^{-3} °C/s, 1.19 × 10^{-3} °C/s and 1.20 × 10^{-3} °C/s. During 4930 ~4943 s, temperatures of FBG1, FBG2 and FBG3 increase by 0.64 °C, 0.75 °C and 0.58 °C, respectively, with increase rates of 4.92 × 10^{-2} °C/s, 5.77×10^{-2} °C/s and 4.46 × 10^{-2} °C/s. The temperature rise of the flashover process is less than that of water deformation process. The duration from discharge to flashover is too short, releasing less heat. The temperature rise speed in the flashover process is more than 10 times that of water deformation process. The heat in this stage mainly comes from the arc discharge. The heat generated per unit time is much higher than that in droplet deformation stage.

3.7. Surface temperature and the UV photon number

Fig. 11 shows the relationship between the maximum surface infrared temperature and the UV photon number. From Fig. 11, the following information can be obtained.

Elongation stage of droplet 1 and droplet 2: surface temperature increases with the rise of UV photon number. UV photon number rises earlier than surface temperature. UV photon number first starts to rise at about 400 s and the rise rate increases at about 600 s. While the surface temperature first starts to rise at about 600 s.

Elongation and movement stage of droplet 3: The surface infrared temperature rises accompanied with oscillation. The curve of UV photon number oscillates but does not increase significantly.

Corona stage: before the corona, UV photon number increases rapidly from 4820 at about 3470 s to 23,400 at about 4010 s. While the surface infrared temperature changes little in this stage. The reason has been described in Section 3.3. The UV photon number in this process is affected by the discharge between the high-voltage electrode and the high-voltage wire. UV photon number begins to increase rapidly at about 4110 s. The surface temperature increases rapidly from 29.1 °C to 30.4 °C at 4140 ~4400 s. At 4420 s, corona occurs and photon number increases rapidly from 18,540 to more than 30,000. Then, surface temperature starts to increase rapidly at about 4560 s.

Table 5
Interface temperature change in the process of droplet deformation and flashover.

Physical process		Droplet deformation	Flashover
Maximum interface temperature rise / °C	FBG1	1.20	0.64
	FBG2	0.85	0.75
	FBG3	0.86	0.58
Rate of interface temperature rise / °C s^{-1}	FBG1	1.68 × 10^{-3}	4.92 × 10^{-2}
	FBG2	1.19 × 10^{-3}	5.77×10^{-2}
	FBG3	1.20 × 10^{-3}	4.46 × 10^{-2}

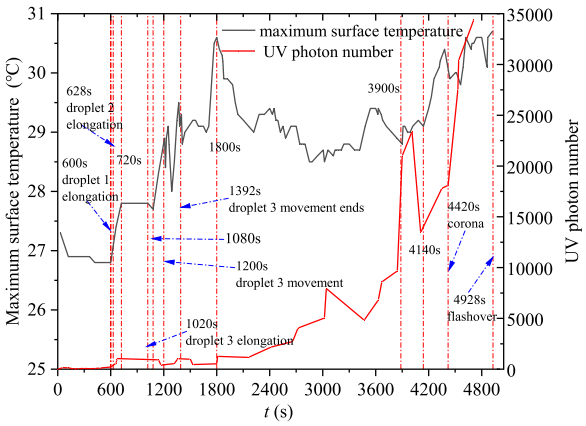


Fig. 11. Maximum surface temperature and UV photon number.

3.8. Surface temperature and interface temperature

It can be seen from Fig. 9 and Fig. 10 that there is a good correlation between the temperature of silicone rubber-epoxy resin interface and the maximum surface infrared temperature. Interface temperature of FBG1 and the maximum surface infrared temperature is described in Fig. 12. The starting time of interface temperature rise lags significantly behind surface temperature rise, and the temperature rise is lower than the surface temperature. The analysis suggests that heat dissipation and time lag occur during the heat transfer from the surface to the interface.

There are brief temperature drops in the rise process of surface temperature and interface temperature. A brief temperature rise process also occurs during the temperature decrease. In AC electric fields, water droplets oscillate, elongate, distort and move throughout the experiment. The length of water droplets and the length of the dry band are always changing. At the same time, water evaporation on the specimen surface and evaporation rate is always in progress and changing. As the experiment progresses, applied voltage continues to rise and the electric field is constantly changed. These changes lead to the change in surface heat generation and heat dissipation speed. Therefore, surface infrared temperature and interface temperature oscillate during the test. Theoretical analysis of heat generation on the specimen surface has been given in Section 4.3.

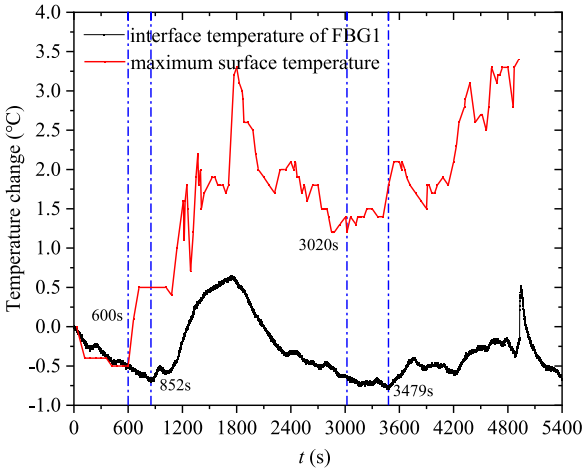


Fig. 12. Variation of interface temperature and surface temperature of hydrophobic silicone rubber.

4. Discussion

4.1. Formation mechanism of high temperature points on the hydrophobic surface

Formation mechanism of high temperature points on hydrophilic insulator surface: pollution of any two positions on the insulator surface is impossible be identical, so can the wetting degree of pollution. Consequently, the resistance of pollution is uneven. The positions with large resistance generate more heat, forming dry bands and high temperature points [27]. As for the clean surface of hydrophobic silicone rubber, the area between water droplets can be regarded as dry bands with higher resistance. While, high temperature points only appear on the area near some water droplets. Obviously, the formation mechanism of high temperature points on the hydrophilic surface is not applicable to the hydrophobic surfaces. In this paper, the formation mechanism of high temperature points on the hydrophobic surface is described as follows.

The existence of water droplets on the silicone rubber surface leads to the distortion of the electric field near the water droplets. The size and shape of water droplets will affect the electric field distribution. The relationship between electric field strength E and surface current density J of hydrophobic silicone rubber specimen is

$$J = \sigma E \tag{2}$$

where σ denotes electrical conductivity.

The relationship between the surface current I and current density is

$$I = JS \tag{3}$$

where S denotes the cross-sectional area of the current channel.

According to Joule's law, the calorific value Q is

$$Q = I^2Rt = \sigma E^2 Slt \tag{4}$$

where l is the length of the current channel and V is the volume of the current channel.

The heating power P per unit volume is

$$P = \sigma E^2 \tag{5}$$

Four identical water droplets are placed on the surface of hydrophobic silicone rubber. The electric field distribution along the symmetrical centerline of the specimen is shown in Fig. 13. The electric field inside the water droplet (conductor) is close to 0 [28]. The electric field strength of the clean surface between water droplets is much higher than that of water droplets. Significant distortion of electric field occurs at the junction of water droplets, silicone rubber surface and air. According to Formula (5), the heating power P at high field strength is higher than that at low field strength. The high temperature point first appears at the position with high electric field strength. This conclusion is supported by the location of the infrared high temperature point in Fig. 8.

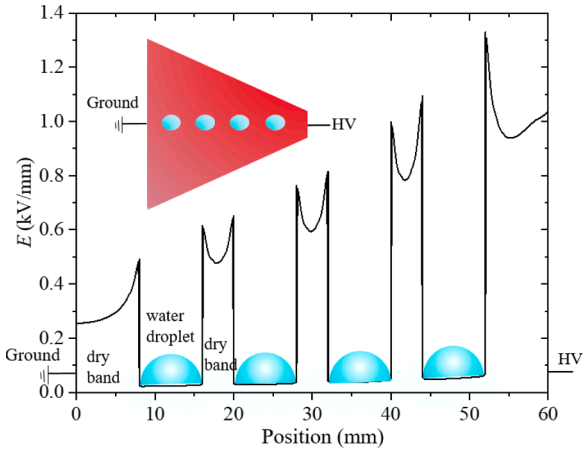


Fig. 13. The electric field distribution of water droplets on the hydrophobic of surface of silicone rubber.

Formula (5) is the same as eddy current heating formula [29], indicating that the heat generation mechanism on the hydrophobic surface of silicone rubber may be the same as eddy current heating.

4.2. High temperature point and droplet elongation

In AC electric field, water droplets on the hydrophobic silicone rubber surface deform dynamically. High temperature points usually appear on the specimen surface near the elongated water droplet. In order to explore the relationship between the elongation of water droplet and high temperature points, the following test was carried out. Semicircular water droplets and an artificially elongated droplet along the electric field were placed on the silicone rubber surface. Fig. 14 shows the infrared temperature on the specimen surface under the applied voltage.

The position where the high temperature point first appears is not near the artificially elongated droplet, but the droplet which is adjacent to the high voltage electrode and is stretched by the electric field. As can be seen from Fig. 13, from the high voltage electrode to the grounding electrode, the electric field strength at the junction of the droplet, silicone rubber surface and air gradually decreases. The artificially elongated droplet in Fig. 14 enhances the electric field near the droplet. While, it may still be lower than the electric field nearby the high voltage electrode. Consequently, the high temperature point does not appear at the position near the artificially elongated droplet. The deformation and elongation of water droplets are the joint effect of electric field force and surface tension. The electric field force makes the water droplets elongate, while the surface tension hinders the elongation of water droplets [3]. The force equilibrium of the droplet with higher contact angle and electric field strength is more easily broken. Then it will elongate. As is shown in Fig. 14, the droplet near the high voltage electrode elongates in electric fields. The elongation of the droplet further enhances the high electric field strengthen. The infrared high temperature point eventually appears on the surface of high electric field strength. There is no high temperature point near the artificially elongated droplet. This may be because the artificially elongated water droplet enhanced the electric field nearby, but the electric field is not the maximum field strength on the specimen surface. The above test results further verify the formation mechanism of high temperature points given in Section 4.3, that is, heat production is proportional to the square of the electric field strength.

Surface tension γ of water droplets is

$$\gamma = \gamma_0(1 + kT) \tag{6}$$

where T denotes the temperature, γ_0 denotes the surface tension at the critical temperature T_0, k denotes the temperature coefficient of surface tension. The increase of temperature at the high temperature side leads to the change of surface tension and the elongation of water droplets.

4.3. Electrothermal synergistic mechanism of high temperature points

According to formula (6), high temperature will promote the deformation and elongation of water droplets. The droplet in Fig. 13 was elongated to obtain the electric field distribution before and after the elongation, as shown in Fig. 15. The elongation of water droplet will increase the electric field strength near the elongated droplet. According to formula (5), the increase of electric field strength will lead to the increase of heat production and temperature. As a consequence, the electric field strength, temperature and droplet elongation promote each other.

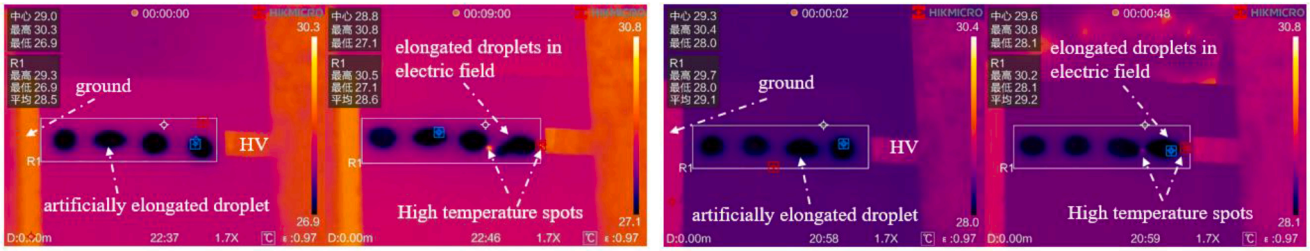


Fig. 14. Surface infrared temperature on the silicone rubber with an artificially elongated droplet. (a) The third on the right is the artificially elongated droplet, (b) The second on the right is the artificially elongated droplet.

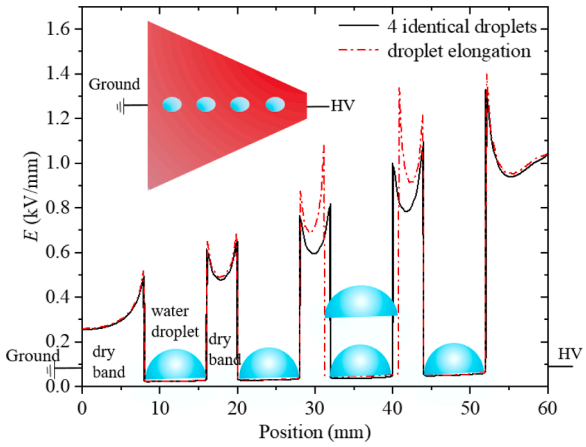


Fig. 15. The electric field distribution of water droplets on the hydrophobic of surface of silicone rubber when droplet is elongated.

5. Conclusion

In this paper, separated water droplets were set on the specimen surface of hydrophobic silicone rubber. During dynamic deformation and flashover of water droplets, visible image of water droplets, UV photon number, leakage current, surface infrared temperature and interface grating temperature were measured. The main conclusions are as follows:

(1) The surface infrared temperature of hydrophobic silicone rubber is affected by the state of surface water droplets. When the water droplet is elongated, surface temperature increases and a high temperature point may ultimately appear near the elongated water droplet.

(2) The interface grating temperature of hydrophobic silicone rubber specimen can reflect the state of surface water droplets. When water droplet deformation and flashover discharge occur, the starting point of interface temperature rise lags behind the surface temperature. The interface temperature rise is relatively low. The interface temperature rise rate with significant difference can be used to distinguish the droplet deformation and the flashover discharge. In the test, the temperature rise rate during water droplet deformation is below 1.68×10^{-3} °C/s, the temperature rise rate during flashover is above 4.46×10^{-2} °C/s.

(3) Formation mechanism of high temperature points, which appear on the hydrophobic silicone rubber surface during the deformation of water droplets, was proposed. The heating power of the silicone rubber surface is proportional to the square of the electric field strength. The high temperature point first appears on the surface with high field strength nearby the elongated water droplet.

(4) The elongation of water droplets contributes to the increase of electric field and heating power, resulting in the occurrence of high temperature point. High temperature further promotes the elongation of water droplets.

Funding

This research was funded by the National Natural Science Foundation of China (52177142) and China Postdoctoral Science Foundation (2021M691056).

Credit author statement

We would like to submit the enclosed manuscript entitled "***A method for detecting conductive droplet deformation and flashover using interface temperature based on electrothermal synergistic mechanism***", which we wish to be considered for publication in ***Electric Power Systems Research***. No conflict of interest exits in the submission of this manuscript, and this manuscript is approved by all authors for publication. I would like to declare on behalf of my co-authors that the work described was original research that has not been published previously, and not under consideration for publication elsewhere, in whole or in part. All the authors listed have approved the manuscript that is enclosed.

Declaration of Competing Interest

We declare that we do not have any commercial or associative interest that represents a conflict of interest in connection with the work submitted.

Data availability

Data will be made available on request.

References

[1] F. Aouabed, A. Bayadi, R. Boudissa, Flashover voltage of silicone insulating surface covered by waterdroplets under AC voltage, Electr. Power Syst. Res. 143 (2017) 66–72.

[2] S. Mohammadnabi, Kh. Rahmani, Influence of humidity and contamination on the leakage current of 230-kV composite insulator, Electr. Power Syst. Res. 194 (2021), 107083.

[3] Y. Liu, Y.F. Wu, Boxue Du, Dynamic formation mechanism of water droplet and induced surface discharges on silicone rubber composites, High Volt. 4 (1) (2019) 59–64.

[4] Y.K. Lv, J.W. Wang, Q.Z. Song, Y.P. Liu, Effect of water drop on electric field distortion of composite Insulator, Power System Technol. 45 (3) (2020) 1201–1207.

[5] M.H. Nazemi, V. Hinrichsen, Partial discharge inception electric field strength of water droplets on polymeric insulating surfaces, IEEE Trans. Dielectr. Electr. Insul. 22 (2) (2015) 1088–1096.

[6] Y. Liu, X.H. Kong, Y.F. Wu, B.X. Du, Dynamic behavior of droplets and flashover characteristics for CFD and experimental analysis on SiR composites, IEEE Access 7 (2019) 8095–8101.
[7] M.E.A. Slama, A. Beroual, A.M. Haddad, M. Albano, Application of analytical modeling of flashover derived for flat samples to polluted 11-kV SiR insulators, IEEE Trans. Dielectr. Electr. Insul. 29 (4) (2022) 1574–1581.
[8] X.L. Jiang, X.D. Ren, H. Wang, X.B. Han, C.L. Bi, Z.Y. Li, L.D. Hou, Effect of inverted T arrangement on AC pollution flashover characteristics of insulator strings, High Volt. 4 (2) (2019) 97–104.
[9] J.K. Bi, Y.P. Hao, L. Yang, Y. Zheng, L.L. Li, Impact of hydrophobicity on wetting characteristics of composite insulators, IEEE Access 8 (2020) 159316–159323.
[10] W. Cao, H. Feng, H. Xue, W. Shen, L. Zhao, H. Yang, Mechanisms and influence factors of dynamic behavior of water droplets on the composite insulator surface under AC electric field, Progr. Electromagn. Res. Lett. 98 (2021) 9–16.
[11] K. Adamiak, J.M. Floryan, Dynamics of water droplet distortion and breakup in a uniform electric field, IEEE Trans. Dielectr. Electr. Insul. 47 (6) (2011) 2374–2383.
[12] W. Cao, H. Xue, W. Shen, H. Yang, L. Zhao, Y. Wang, The effect of dynamic behaviours of the water droplet on DC/AC flashover performance on silicone rubber surface: experiment, simulation and theoretical analysis, High Volt. 6 (4) (2021) 637–646.
[13] B. Cao, S.C. Shao, X.H. Wu, F.H. Yin, L.M. Wang, M. Farzaneh, Flashover characteristics of a hydrophobic surface covered by water, J. Phys. D Appl. Phys. 54 (7) (2021), 075501.
[14] Y.F. Li, H.Y. Jin, S.C. Nie, P. Zhang, N.K. Gao, Dynamic behavior of water droplets and flashover characteristics on a superhydrophobic silicone rubber surface, Appl. Phys. Lett. 110 (20) (2017), 201602.1-201602.4.
[15] S. Chatterjee, M.H. Nazemi, Influence of viscosity and conductivity of water droplets on partial discharge inception voltages of polymeric insulating surfaces, in: Proc. Int. Conf. Energy, Power Environ., Towards Sustain. Growth (ICEPE), Jun. 2015, pp. 1–4.
[16] G.X. Xu, P.B. McGrath, Electrical and thermal analysis of polymer insulator under contaminated surface conditions, IEEE Trans. Dielectr. Electr. Insul. 3 (2) (1996) 289–298.
[17] J.O. Loberg, E.C. Salthouse, Dry band growth on polluted insulation, IEEE Trans. Dielectr. Electr. Insul. 6 (13) (1971) 136–141.
[18] F. Liang, M. Mark, Z.C. Guan, R.B. Zhang, Formation of dry-band in the process of pollution flashover based on infrared thermal image analysis, High Volt. Eng. 40 (1) (2014) 138–146.
[19] Y.P. Hao, Y. Fu, J. Wei, L. Yang, G.Y. Mao, Z.L. Yang, L.L. Li, Internal temperature detections of contaminated silicone rubber under discharge conditions based on fiber bragg gratings, IEEE Access 7 (2019) 161167–161174.
[20] Y.P. Hao, J.K. Bi, Q. Wang, L. Yang, Interface temperature evolution exposed to arc discharges occurred on the uniform moist pollution layer of composite insulators based on interface fibre Bragg gratings, High Volt. 7 (4) (2022) 763–770.
[21] Y.P. Hao, J.K. Bi, Q. Wang, J. Wei, Y.W. Chen, L. Yang, Method of quasi-distributed interface fiber Bragg gratings monitoring dry band arc on the moist pollution layer of composite insulators, Electr. Power Syst. Res. 209 (2022), 107956.
[22] A. Xiao, S.M. Rowland, X. Tu, J.C. Whitehead, Thermal features of low current discharges and energy transfer to insulation surfaces, IEEE Trans. Dielectr. Electr. Insul. 21 (6) (2014) 2466–2475.
[23] G.X. Xie, J.B. Luo, Y. Yang, D. Guo, L.N. Si, Water droplets on a hydrophobic insulator surface under high voltages: a thermal perspective, Appl. Phys. Lett. 101 (2012), 131602.
[24] G.X. Xie, F. He, X. Liu, L.N. Si, D. Guo, Sessile multidroplets and salt droplets under high tangential electric fields, Sci. Rep. 6 (2016) 25002.
[25] IEC 60507:1991, “Artificial pollution tests on high-voltage insulators to be used on a.c. systems”.
[26] S. Du, W. Cai, H.M. Deng, S. Wen, W. Deng, P. Xiong, Production and calibration test of the composite insulator with Fiber Bragg Grating embedded, High Volt. Engineering 25 (7) (2012) 2774–2780.
[27] W. Shi, Y.C. Qiu, Zhang Q.G, Fundamentals of High Voltage Engineering, China Machine Press, 2014.
[28] Z.K. Shen, Z.D. Jia, Y.P. Hao, Z.Y. Xin, X.L. Wang, A fabrication method for adaptive dielectric gradient insulating components, High Volt. (2022).
[29] Y.X. Tu, L.S. Liu, C.J. Guo, H.W. Mei, C.L. Cong, L.M. Wang, Active electromagnetic induction thermography for conductive defects detection on composite insulators, Proc. CSEE 41 (7) (2021) 2565–2576.